

^{129}Xe NMR of Mesoporous Silicas

T. Pietraß* and J. M. Kneller

Department of Chemistry, New Mexico Tech, Socorro, NM 87801.

R. A. Assink and M. T. Anderson‡

Sandia National Laboratories, Albuquerque, NM 87185.

RECEIVED**APR 26 1999****OSTI**

Abstract

The porosities of three mesoporous silica materials were characterized with ^{129}Xe NMR spectroscopy. The materials were synthesized by a sol-gel process with $r = 0, 25,$ and 70% methanol by weight in an aqueous cetyltrimethylammonium bromide solution. Temperature dependent chemical shifts and spin lattice relaxation times reveal that xenon does not penetrate the pores of the largely disordered ($r = 70\%$) silica. For both $r = 0$ and 25% , temperature dependent resonances corresponding to physisorbed xenon were observed. An additional resonance for the $r = 25\%$ sample was attributed to xenon between the disordered cylindrical pores. 2D NMR exchange experiments corroborate the spin lattice relaxation data which show that xenon is in rapid exchange between the adsorbed and the gas phase.

*Author to whom correspondence should be addressed.

‡Current address: Advanced Materials Technology Center, 3M Center, Building 201-4N-01, St. Paul, MN 55144-1000.

DISCLAIMER

Portions of this document may be illegible in electronic image products. Images are produced from the best available original document.

DISCLAIMER

This report was prepared as an account of work sponsored by an agency of the United States Government. Neither the United States Government nor any agency thereof, nor any of their employees, make any warranty, express or implied, or assumes any legal liability or responsibility for the accuracy, completeness, or usefulness of any information, apparatus, product, or process disclosed, or represents that its use would not infringe privately owned rights. Reference herein to any specific commercial product, process, or service by trade name, trademark, manufacturer, or otherwise does not necessarily constitute or imply its endorsement, recommendation, or favoring by the United States Government or any agency thereof. The views and opinions of authors expressed herein do not necessarily state or reflect those of the United States Government or any agency thereof.

Introduction

The development of a novel group of mesoporous materials, denoted M41S and related periodic porous oxides,¹ has generated a great deal of interest due to their highly uniform pore sizes. They have great potential as catalysts, chromatographic supports, separation materials, photonic crystals, and in electronic devices.² The large pore size, surface area, and easy functionalization of the silica wall provide further applications as supports for chemical and biological reactions.³ Recently, it has been shown that these materials can be synthesized over several length scales by a combination of micromolding, templating and cooperative assembly of inorganic sol-gel species, substantially widening their range of applications.⁴ Ordered meso- and macroporous silica systems are synthesized by introducing templates into the reaction mixture. Two main approaches are at hand for the construction of templated silica frameworks: (i) amphiphilic surfactant molecules or polymers serve as templates that interact with the silica precursors via electrostatic, van der Waals, and hydrogen bonding interactions, and (ii) organic ligands covalently bonded to the silica precursors can be used as templates.⁵ The former approach yields a large variety of *ordered* materials depending on the nature of the template.

Cetyltrimethylammonium bromide (CTAB) is a proven templating agent. It forms micelles in aqueous solution. The presence of a cosolvent influences the degree of aggregation of CTAB, which affects the template size, unit cell size, and pore size of the product.⁶ It has been shown that an increasing amount of methanol as a cosolvent increases the critical micelle concentration.⁷ If the weight percentage, r , of methanol in aqueous surfactant solution exceeds 60%, all surfactant is present in the form of free surfactant or small aggregates prior to the addition of the silica source. This leads to a decrease in long-range order of the final product. Whereas for $r = 0$ to 25% ordered hexagonal mesophases have been confirmed with powder X-ray diffractometry, a larger value of r leads to a disordered arrangement of cylindrical pores. For $r \geq 70\%$, disordered 'wormlike' structures have been observed.⁸ Nitrogen sorption studies indicate an increase in pore diameter and periodic porosity with decreasing r .⁸ Scanning electron microscopy revealed particle sizes in the submicron to micron range. For silicas with $r = 0$ to 25%, the roughly micron sized particles are aggregates of smaller (ca. 0.02 μm diameter) primary particles, which contain a periodic hexagonal array of 2 to 3 nm particles. Here, the entire volume of the micron sized particle should be accessible to gaseous adsorbates. Contrary, for $r \geq 70\%$, the arrangement of the primary particles is less ordered. Pores may be discontinuous, faulted, or even collapsed. The interparticle space between the primary particles is filled, so that adsorbates are expected to penetrate only the outermost layer of primary particles, i.e., up to a depth of about 0.02 to 0.05 μm .⁸ Whereas pore size, pore volume, and surface area

are in principle accessible from powder X-ray diffractometry and nitrogen sorption, the connectivity and structure of the pores is unknown.

In this work, we study the porosity of three silica samples prepared with methanol as a cosolvent in different proportions ($r = 0, 25, 70\%$ by weight) using ^{129}Xe NMR spectroscopy. Models have been developed to derive the pore size distribution from ^1H NMR spin lattice relaxation times of water confined in the porous solids,^{9,10} but xenon interacts less strongly with the silica surface, does not affect the number of silanol bearing silicons, and samples a larger volume than water on a given timescale. With a van der Waals diameter of 4.4 Å, xenon will diffuse readily into the mesopores, given that the pore access is not restricted. The high sensitivity of the xenon chemical shift to its chemical environment provides additional information to NMR relaxation data.

Experimental

The silica materials were synthesized by a sol-gel process with CTAB as micelle forming agent and r varying between 0 and 70%. The synthesis is described in detail in ref. [8]. The results from structural characterization other than NMR are summarized in Table 1.

For preliminary ^{129}Xe NMR experiments, the xenon was adsorbed onto the untreated silica samples (as received). This is justified when considering potential industrial applications which require usage of the sample 'as is'. Then, two sets of dehydrated samples with a high and low pressure of xenon, respectively, were prepared from each of the silica materials. These samples were heated under vacuum (10^{-4} torr) over a period of 4 h to 400°C, were kept at this temperature for 4 to 8 h, and were allowed to cool to ambient temperature over a period of 5 h. Subsequently, for the set of low xenon pressure (LP) samples, $1.2 \cdot 10^{-4}$ mol of xenon (enriched to 80% in ^{129}Xe) was condensed onto the silica, and the sample tube was flame sealed under exclusion of air. A 5 mm outer diameter glass tube with a wall thickness of ca. 1 mm was used. 0.0546 g of silica 1, 0.0856 g of silica 2, and 0.0639 of silica 3 were weighed in. The sealed sample tubes measured about 6 cm in length, and about half of the volume was filled by the loosely packed powder. For an empty sample tube, this would correspond to a pressure of 5 to 6 atm. The equilibrium xenon gas densities were determined from the chemical shift of the free gas resonance.¹¹ These shifts were measured by turning the sample tubes upside-down, so that the region of the sample tube that did not contain any powder was inside the NMR pick-up coil.¹² However, the chemical shift of the xenon gas in this region may nevertheless be affected by surface interactions, as the observed spin lattice relaxation times were much shorter (*vide infra*) than those expected for the free gas of $10^3 - 10^4$ s.^{13,14} The freshly sealed samples were checked for the intensity of the ^{129}Xe NMR signal, and then heated again to 400°C

for 4 h, to facilitate the perfusion of the pores by the xenon.¹⁵ No difference in the chemical shifts nor the spin lattice relaxation times T_1 was observed after heating. These samples will be referred to as x-LP, where x is the silica sample number from Table 1.

The high xenon pressure set of samples (HP) was prepared in an analogous way, but $5.1 \cdot 10^{-4}$ mol of enriched xenon was added to 0.0456 g silica 1, 0.0750 g silica 2, and 0.0735 g silica 3, corresponding to a pressure of about 25 atm. These samples will be referred to as x-HP. Spread out in a monolayer under the assumption of square packing, this amount of xenon will cover an area of 60 m^2 . Thus, there is enough xenon available for a coverage with 1.6 (1-HP), 1.2 (2-HP), and 2.6 (3-HP) monolayers. No difference in the chemical shift nor the spin lattice relaxation times was observed when two of the samples (1-HP and 3-HP) were subjected to a heating procedure (3 h at 300°C) after xenon adsorption. Equilibrium gas densities determined as described above were 2 amagat for the x-LP samples, and 14.4 amagat (1-HP), 13.3 amagat (2-HP), and 15.5 amagat (3-HP), respectively.¹¹

The NMR experiments were carried out on a Bruker MSL-400 NMR spectrometer, with a Larmor frequency of 110.668 MHz for ^{129}Xe . An inverse NMR probe was used with a 90° pulse length of 24 μs . Only the region of the sample tubes containing the powder were in the coil area. Xe gas with 0.3% oxygen was used as an external chemical shift reference.¹¹ ^{29}Si spectra were recorded on a Bruker AMX-400 NMR spectrometer equipped with a CP/MAS probe. Samples weighing between 0.2 and 0.3 g were spun at 4 kHz in 7 mm ceramic rotors. The spectra were referenced by setting the downfield resonance of octakis(trimethylsiloxy)silsesquioxane to 12.5 ppm.

Results

Temperature dependent ^{129}Xe NMR spectra of sample 1-HP are shown in Figure 1. At ambient temperature (293 K), resonances for xenon in the gas phase and for physisorbed xenon are observed at 11.9 and 50.7 ppm, respectively. The chemical shift of the resonance due to physisorbed xenon increases with decreasing temperature. At 200 K, a third resonance at 233 ppm becomes observable which is tentatively assigned to xenon in the liquid phase. The phase diagram for xenon predicts condensation at 200 K at a pressure of 4.1 atm.¹⁶ At 164 K, these resonances merge, and at 155 K, a resonance at 298 ppm appears which is most likely due to solid xenon. The chemical shifts of the physisorbed xenon are summarized in Figure 2 (x-HP) and Figure 3 (x-LP). For the 2-HP sample, a similar temperature dependence as for 1-HP is observed, whereas 3-HP shows a very different behavior. Here, the only indication of physisorbed xenon at ambient temperature is a shoulder located on the downfield side of the gas resonance. At 220 K, a narrow

resonance at 219 ppm appears, which shifts further downfield when lowering the temperature. This resonance is assigned to xenon in the liquid phase which requires an equilibrium pressure of 9.4 atm at this temperature.¹⁶ At 160 K, the resonance typical for solid xenon is observed. 3-LP shows a similar chemical shift dependence as 3-HP. The 2-HP sample has an additional resonance a few ppm downfield of the gas resonance. This resonance shifted further downfield upon cooling (29 ppm at 232 K), and disappeared at 220 K. It is not included in Figure 2.

The chemical shifts and spin lattice relaxation times T_1 for the x-LP samples are summarized in Table 2; the spin lattice relaxation times of x-HP in Table 3. For the x-LP samples, the T_1 s at ambient temperature were also recorded before dehydrating the silica. Due to signal-to-noise constraints, it was not possible to decompose peak components arising from the gas and the adsorbed phase for the x-LP and 3-HP samples. Qualitatively, the peak components seemed to evolve with the same time constant. For the other two x-HP samples, the peak components were well resolved, and individual T_1 s could be determined.

The linewidths of the resonances assigned to physisorbed xenon for 1-HP and 2-HP are shown in Figure 4. For 2-HP (full triangles), a maximum in linewidth is reached at 225 K. The maximum in linewidth for 1-HP is less pronounced at about 240 K. The linewidth of the smaller resonance with a shift close to the gas phase resonance in 2-HP is independent of temperature.

Exchange of xenon in the gas phase with physisorbed xenon was studied with 2D NMR exchange spectroscopy.¹⁷ These experiments were mainly carried out on the 1-HP sample which gave rise to the strongest signals. Crosspeaks were observed at ambient temperature at mixing times of 10 ms, 20 ms, 100 ms, and 500 ms, and at 240 K and 200 K, for a mixing time of 20 ms.

²⁹Si magic angle spinning experiments to determine the Q^3 (silicons with a single hydroxyl group) to Q^4 (siloxane) ratio yielded an estimate for the surface area which is independent of the BET isotherms.^{18,19} For silica 1 and 2, a ratio $Q^3/Q^4 = 1/2$ was found, and for silica 3 $Q^3/Q^4 = 1/1$. This result indicates a larger surface area on silica 3, which is not consistent with the BET data (Table 1). The origin of this discrepancy is not clear, it may be caused by Q^3 in the interior of the silicate rather than on the surface. The ratio Q^3/Q^4 provides an upper limit to the surface area, the actual surface area may be significantly less.

Discussion

a) Pore Penetration and Condensation

For the lower pressure samples x-LP, the chemical shift of the hydrated samples is larger than for the dehydrated samples (Table 2). The water content before dehydration in silica 1, for instance, is sufficient to cover its surface area with about one monolayer of water. Thus, the chemical shift difference is very likely due to removal of physisorbed water in the pores which creates a different chemical environment for the xenon.²⁰ Moreover, the presence of water decreases the pore volume accessible to the xenon,²¹ which also affects the ^{129}Xe NMR chemical shift. This is substantiated by the fact that the spin lattice relaxation times are increasing upon dehydration (Table 2). It is likely that, in the presence of water, the dominant relaxation mechanism for xenon is a dipolar interaction with water protons. Removal of the protons would thus eliminate this relaxation pathway. The samples 1,2-LP exhibit two spectral components a and b which shift significantly upfield upon dehydration (Table 2). Tentatively, these components are assigned to xenon adsorbed inside the pores (component a), and xenon in between the primary particles (component b). The smaller shift in 3-LP indicates less interaction with the silica surface. Upon dehydration, the two spectral components show a shift typical for the free gas.

Within experimental error, no change in the spin lattice relaxation time has been observed for 3-LP after dehydration (Table 2), which indicates that the ^{129}Xe T_1 is not affected by the presence of the water. Most likely, the xenon does not penetrate the pores which host the water before dehydration. The same phenomenon has been observed for xenon in hydrated zeolite NaY.²² The smaller chemical shift of 3-LP than of 1,2-LP further substantiates this possibility. Similarly, in the 3-HP sample, the ^{129}Xe NMR chemical shift is smaller than in the other two HP samples. From the TEM structure analysis, it is expected that the xenon in this sample can only penetrate the surface layer of primary particles in the aggregates. Exchange with xenon in the interparticle space should be very efficient due to the small penetration depth, and the resonance is expected to have a small chemical shift with respect to xenon in the interparticle space.¹² The rather weak intensity also agrees well with the TEM results, since only a small fraction of the particles is accessible to the xenon.

In 3-HP, the T_1 shortens when cooling to 240 K indicating that on average the xenon dwells longer on the silica surface. The same trend would be expected when further lowering the temperature, but the experimental T_1 value at 200 K is actually substantially longer. This is due to the fact that at this temperature the observed resonance originates from liquid xenon. Spin lattice relaxation times for the pure liquid of $1.5 \cdot 10^3$ s have been measured recently for xenon in pyrex glass.²³ The shorter T_1 value for 3-HP suggests

small pools of liquid xenon, where xenon in contact with the silica surface contributes to the observed relaxation time.

For 1,2-HP, the spin lattice relaxation times are decreasing with decreasing temperature. Consistent with this trend (for a relaxation delay $\tau = 4 \text{ s} \ll 5 T_1$), the overall signal intensity is increasing with decreasing temperature. As more and more xenon condenses into the pores, the contribution to T_1 from xenon in the gas phase is diminished, T_1 decreases, and the signal intensity increases. The condensation of xenon in the pores can be monitored through the ratio of the integrals of the gas and adsorbed phase resonance. It is shown for 1-HP in Figure 5 (filled circles). With the appearance of the liquid phase, the intensity of the adsorbed phase resonance is decreasing (unfilled circles).

b) Xenon Mobility and Adsorption Sites

Within experimental error, the spin lattice relaxation times for x-HP are the same for the adsorbed and gas phase resonances (Table 3), indicating a rapid exchange between the two phases. This was confirmed with 2D NMR exchange spectroscopy through the presence of crosspeaks at mixing times as low as 10 ms. A self-diffusion coefficient on the order of $10^{-9} \text{ m}^2/\text{s}$ has been measured for xenon in zeolite with a loading of one xenon atom per supercage.²⁴ Using this number for an estimate, a xenon atom will diffuse about $2.5 \text{ }\mu\text{m}$ in 10 ms. Thus, it is not unreasonable to assume that a xenon atom can traverse an entire micron-long particle during a mixing time of 10 ms.

Since at the onset of the appearance of the resonance for liquid xenon also the much broader resonance for adsorbed xenon is observable, it seems plausible, that the different phases are present simultaneously in different sample regions. In the x-HP samples, the amount of xenon is sufficient to reach monolayer coverage before all of the xenon has been adsorbed. With more surface area and pore volume available in 1-HP, this point is reached at a higher temperature, and is probably equivalent to the maximum observed in Figure 4. Instead of an idealized monolayer, xenon island formation is a more realistic scenario. When more xenon is adsorbed onto those islands, pools of liquid may form at different sites and on different timescales, which would explain the coexistence of the two phases.

Before the onset of liquid formation at a specific site, more and more xenon atoms have other xenon atoms as neighbors, leading to a more homogeneous chemical environment of the xenon and a decrease in linewidth (Figure 4). The linewidths on the order of kHz may be caused by ^{129}Xe - ^{129}Xe dipolar interactions, chemical shift anisotropy, or a heterogeneity of the adsorption sites within the pores. Such a heterogeneity may be caused by a pore size distribution. The temperature dependence of the 1D linewidth indicates a motional process be involved. Therefore, we conclude that the linewidths are most likely

dominated by a heterogeneity of the adsorption sites. The exchange between different xenon positions within an island must be slower than 0.16 ms for a linewidth of 1 kHz. For the 1-HP sample, the xenon seems to penetrate easily the hexagonally arranged cylindrical pores. The highly ordered system offers mainly adsorption sites inside the pores to the xenon. These must be quite homogeneous, as the linewidth of this resonance is not changing significantly with decreasing temperature. The presence of a second resonance for physisorbed xenon at low chemical shifts in 2-HP must arise from a different type of adsorption site, such as in between the more disordered primary particles. The spatial confinement should be less restricted than inside the pores, and the chemical shift should be closer to the gas resonance, which is in agreement with the experimental result.

c) Pore Size

Attempts have been made to correlate pore size with ^{129}Xe NMR chemical shift data.²⁵ Cheung²⁶ derived a theoretical prediction on the non-linear temperature dependence of the ^{129}Xe chemical shift. His simplest model uses a square-well potential to describe the adsorption sites of a xenon atom in a layerlike pore. Fitting the temperature dependent chemical shift data $\sigma(T)$ to equation (1)

$$\sigma(T) = \frac{c \cdot \varepsilon}{1 + F \cdot \exp[-\varepsilon / kT]}, \quad \text{where} \quad F = \frac{L - 2r_{\text{Xe}}}{2l \cdot m - 1} \quad (1)$$

yields a value for L , which is related to the mean free path λ of xenon by $L = r_{\text{Xe}} + 2\lambda$. The mean free path can be judged as a measure of pore size. Molecular Dynamics calculations,²⁷ however, show that xenon in zeolites moves about preferentially in close proximity to the pore walls, which questions the significance of the parameter L as a measure of pore size. F is a geometrical factor which depends on the radius of the xenon atom, r_{Xe} , l is the width of the potential, and m is equal to 1, 2, or 3, depending on the dimensionality of the pore. ε is the depth of the potential well.

Equation (1) is valid for pressures where the xenon-xenon interaction is not important. Our samples are beyond this regime. Therefore, the data for x-LP and x-HP were linearly extrapolated to zero pressure. The resultant data points were fitted to equation (1). The result for $x = 1$ and 2 is shown in Figure 6. For $x = 3$, the number of data points was not sufficient. The solid (silica 2) and dashed (silica 1) line in Figure 6 were obtained when setting the dimensional factor $m = 2$ (cylindrical pores). These results are summarized in Table 4. For cylindrical pores, the pore diameter d equals twice the hydraulic pore diameter d_h ($d = 2 d_h$). For samples 1 and 2, the hydraulic pore diameter obtained from the fits

shown in Figure 6 thus corresponds to 18 Å and 19 Å, respectively. The estimates from the ^{129}Xe NMR results are in reasonable agreement with the BET and X-ray data (Table 1). However, contrary to these data, the ^{129}Xe NMR results suggest a smaller or equal pore size for $r = 0\%$ than for $r = 25\%$. This is not expected, as the template and thus the pore size should be largest without a cosolvent (silica 1). Moreover, the ^{129}Xe NMR data require an *a priori* assumption about the pore geometry. The linear pressure dependence of the chemical shift is an arbitrary assumption, and allows one to judge the results from the fits only as a crude test to the applicability of the model. These results clearly show the need for a better model. Due to the long spin lattice relaxation times, chemical shift data at low pressures have to be collected using optically polarized xenon.²⁸ This work is currently in progress.

Conclusions

Our data show that a mesoporous silica prepared with 70% of methanol as a cosolvent in the surfactant solution possesses pores which are barely accessible to the xenon. This conclusion cannot be drawn from the nitrogen sorption studies, and demonstrates the usefulness of xenon in combination with ^{129}Xe NMR as a probe for studying internal cavities. For smaller amounts of methanol, a porous silicate structure results that can easily be penetrated by xenon. The timescale for exchange of xenon in the interparticle space with xenon in the pores is very fast; the exchange occurs in less than 10 ms. The easy accessibility of the pores underlines the application of these materials as catalyst supports and gas separation materials.

Acknowledgments

Helpful discussions with Dr. J. Brinker, Dr. A. Labouriau, and Dr. W. L. Earl are gratefully acknowledged. This work was supported by the Director, Office of Energy Research, Office of Basic Energy Sciences, Materials Sciences Division, U.S. Department of Energy, under contract No. DE-AC04-94AL85000 in the framework of the SURP (Sandia University Research Program) program.

Sandia is a multiprogram laboratory operated by Sandia Corporation, a Lockheed Martin Company, for the United States Department of Energy under contract DE-AC04-94AL85000.

References

- (1) Kresge, C. T.; Leonowicz, M. E.; Roth, W. J.; Vartuli, J. C.; Beck, J. S. *Nature* **1992**, *359*, 710.
- (2) Behrens, P.; Stucky, G. D. *Angew. Chem. Int. Ed. Engl.* **1993**, *32*, 696-699.
- (3) Zhao, D.; Yang, P.; Huo, Q.; Chmelka, B. F.; Stucky, G. D. *Curr. Opin. Solid Mater.* **1998**, *3*, 111-121.

- (4) Yang, P.; Deng, T.; Zhao, D.; Feng, P.; Pine, D.; Chmelka, B. F.; Whitesides, G. M.; Stucky, G. D. *Science* **1998**, *282*, 2244-2246.
- (5) Raman, N. K.; Anderson, M. T.; Brinker, C. J. *Chem. Mater.* **1996**, *8*, 1692.
- (6) Anderson, M. T.; Martin, J. E.; Odinek, J. G.; Newcomer, P. P. *Chem. Mater.* **1998**, *10*, 311-321.
- (7) Anderson, M. T.; Sawyer, P. S.; Rieker, T. *Micro. and Mesoporous Mater.* **1998**, *20*, 53-65.
- (8) Anderson, M. T.; Martin, J. E.; Odinek, J. G.; Newcomer, P. P. *Chem. Mater.* **1998**, *10*, 1490-1500.
- (9) Schmidt, R.; Hansen, E. W.; Stöcker, M.; Akporiaye, D.; Ellestad, O. H. *J. Am. Chem. Soc.* **1995**, *117*, 4049.
- (10) Alba, M. D.; Becerro, A. I.; Klinowski, J. *J. Chem. Soc., Faraday. Trans.* **1996**, *92*, 849.
- (11) Jameson, C. J.; Jameson, A. K.; Cohen, S. M. *J. Chem. Phys.* **1973**, *59*, 4540.
- (12) Jameson, C. J.; Jameson, A. K.; R. E. Gerald, I.; Lim, H.-M. *J. Phys. Chem. B* **1997**, *101*, 8418-8437.
- (13) Torrey, H. C. *Phys. Rev.* **1963**, *130*, 2306.
- (14) Hunt, E. R.; Carr, H. Y. *Phys. Rev.* **1963**, *130*, 2302.
- (15) Larsen, R. G.; Shore, J.; Schmidt-Rohr, K.; Emsley, L.; Long, H.; Pines, A.; Janicke, M.; Chmelka, B. F. *Chem. Phys. Lett.* **1993**, *214*, 220.
- (16) *Edelgase*; Gmelin, L., Ed.; Verlag Chemie: Leipzig-Berlin, 1924.
- (17) Jeener, J.; Meier, B. H.; Bachmann, P.; Ernst, R. R. *J. Chem. Phys.* **1979**, *71*, 4546.
- (18) Davis, P. J.; Brinker, C. J.; Smith, D. M.; Assink, R. A. *J. Non-Cryst. Solids* **1992**, *142*, 197.
- (19) Davis, P. J.; Deshpande, R.; Smith, D. M.; Brinker, C. J.; Assink, R. A. *J. Non-Cryst. Solids* **1994**, *167*, 295.
- (20) Pietraß, T.; Bifone, A.; Pines, A. *Surf. Sci.* **1995**, *334*, L730.
- (21) Barrie, P. J.; Klinowski, J. *Prog. NMR Spec.* **1992**, *24*, 91.
- (22) Ripmeester, J. A.; Ratcliffe, C. I. *Anal. Chim. Acta* **1993**, *283*, 1103.
- (23) Sauer, K. L.; Fitzgerald, R. J.; Happer, W. *Chem. Phys. Lett.* **1997**, *277*, 153.
- (24) Karger, J.; Bar, N.-K.; Heink, W.; Pfeifer, H.; Seiffert, G. *Z. Naturforsch.* **1995**, *50a*, 186-190.
- (25) Demarquay, J.; Fraissard, J. *Chem. Phys. Lett.* **1987**, *136*, 314.
- (26) Cheung, T. T. P.; Chu, P. J. *J. Phys. Chem.* **1992**, *96*, 9551.
- (27) Yashonath, S.; Santikary, P. *J. Phys. Chem.* **1993**, *97*, 3849.

(28) Pietraß, T.; Gaede, H. C. *Adv. Mat.* **1995**, *7*, 826.

Tables

Table 1

sample	r [wt %]	a [Å]	surface area [m ² /g]	pore volume [cm ³ /g]	hydraulic pore diameter [Å]
1	0	38.7 (3)	844	0.66	16
2	25	35.6 (3)	650	0.39	12
3	70	<34	317	0.20	13

Table 2

sample	shift [ppm] before dehydration		shift [ppm] after dehydration		T ₁ [s] before dehydration	T ₁ [s] after dehydration
	component a	component b	component a	component b		
1-LP	71	47	30	13	6.5 ± 1.0	48 ± 14
2-LP	52	35	27	8	3.2 ± 0.5	19 ± 4
3-LP	33	32	4	2	31 ± 11	34 ± 7

Table 3

sample		T ₁ (298 K) [s]	T ₁ (240 K) [s]	T ₁ (200 K) [s]
1-HP	gas	18 ± 1	5.1 ± 0.9	
	ads.	15 ± 1	6.9 ± 1.0	2.7 ± 0.9
2-HP	gas	70 ± 14	35 ± 16	
	ads.	53 ± 5	35 ± 16	15 ± 3
3-HP	gas/ads.	52 ± 8	19 ± 5	
	liq.			44 ± 7

Table 4

sample	m	ε [kJ/mol]	l [Å]	L [Å]	λ [Å]
1	2	6.5	0.06	74	35
2	2	6.5	0.06	80	38

Table Captions

Table 1: Structural data for the mesoporous silica samples. r is the amount of methanol added to the aqueous surfactant (CTAB) solution expressed as weight %, a is the unit cell constant. The surface area A was determined from nitrogen adsorption isotherms at 77 K. The pore volume V_p is determined from the density, and the hydraulic pore diameter $d_h = 2 V_p/A$. All data from ref. [8].

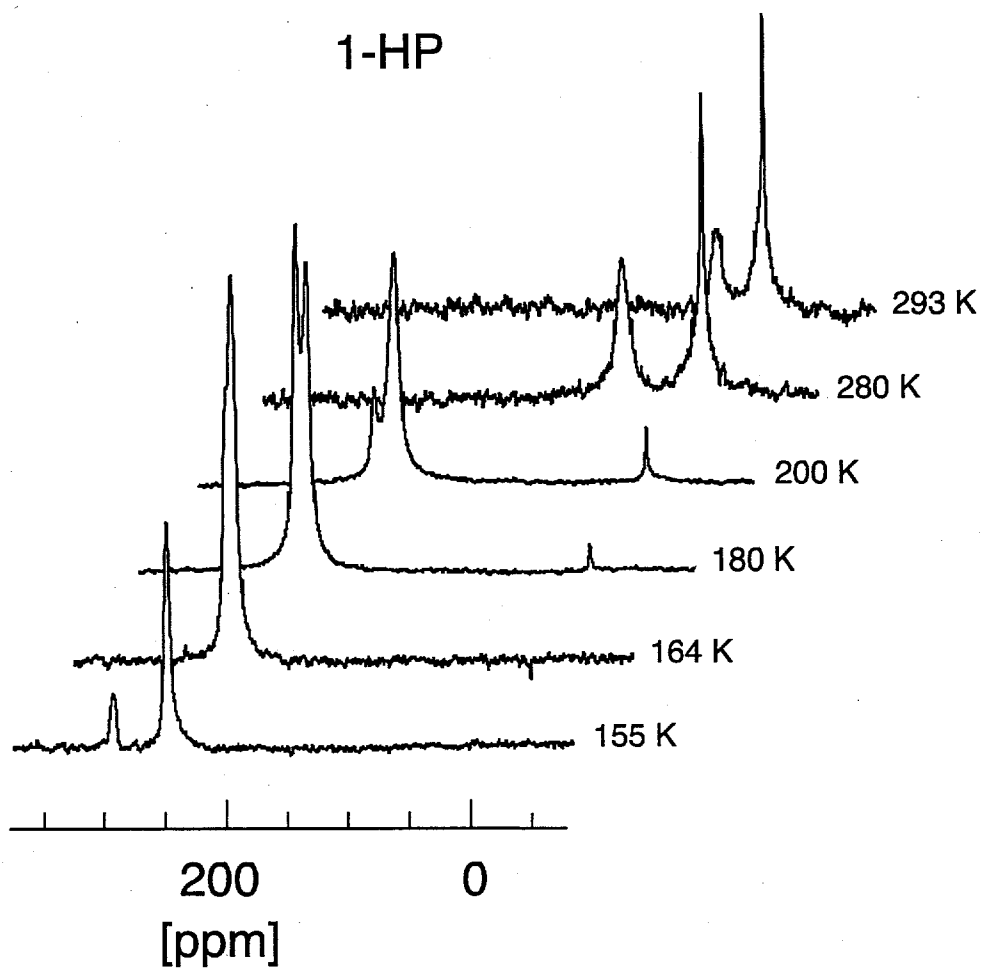
Table 2: ^{129}Xe NMR chemical shifts and T_1 s before and after dehydration of the lower pressure samples x-LP.

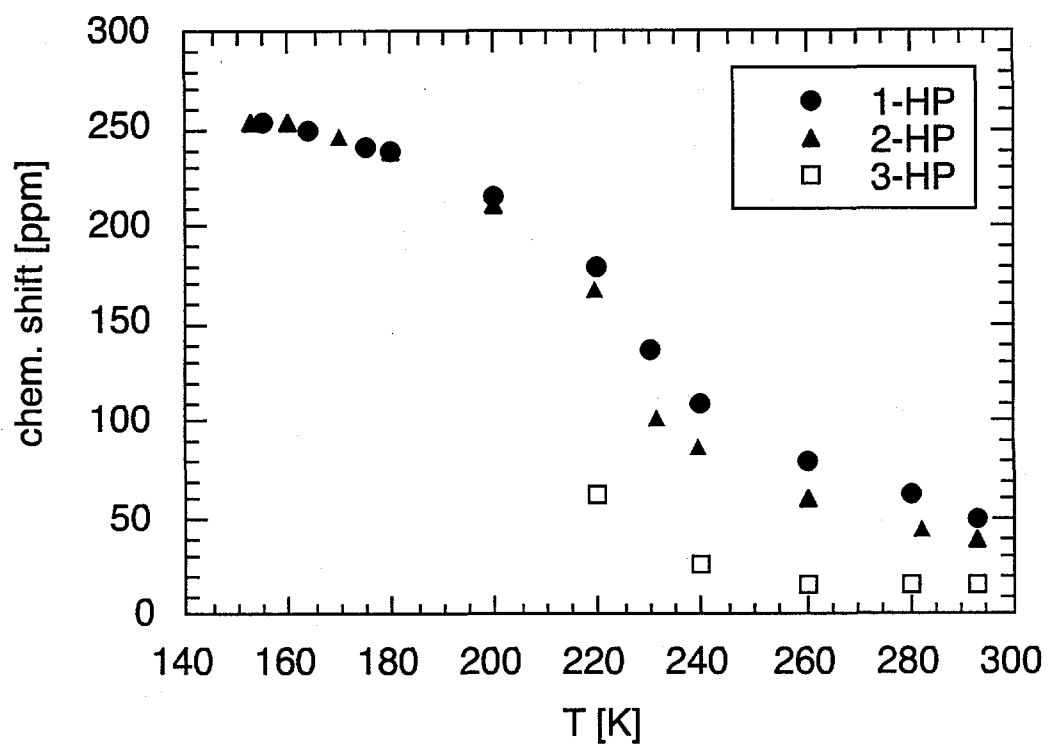
Table 3: ^{129}Xe NMR spin lattice relaxation times of the higher pressure samples x-HP.

Table 4: Results of the fits of the temperature dependent chemical shift data of the resonance for physisorbed xenon of silica 1 and 2 to equation (1). The chemical shift data have been linearly extrapolated to zero pressure from the data in Figures 2 and 3. These data and the fits for $m = 2$ are shown in Figure 6.

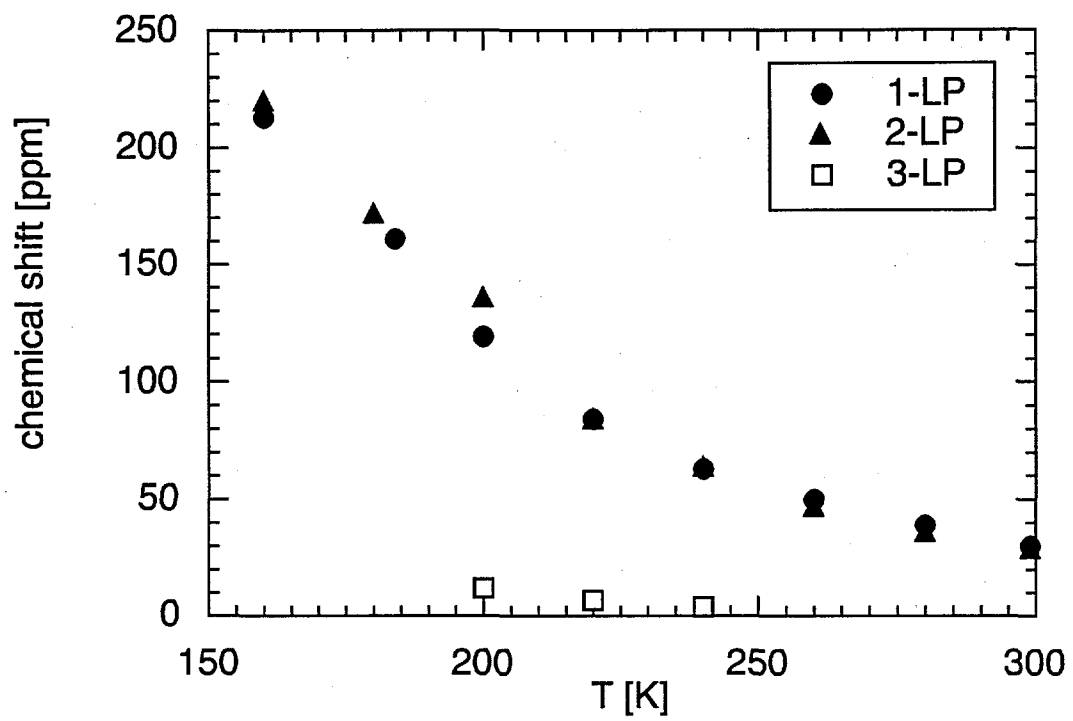
Figure Captions

- Fig. 1: Temperature dependent ^{129}Xe NMR spectra of 1-HP. The spectra were recorded with a 10 μs pulse length and a relaxation delay of 4 s. Number of transients: 2048 (293 K - 180 K), 256 (164 K), 128 (155 K).
- Fig. 2: Temperature dependent ^{129}Xe NMR chemical shifts of the resonance assigned to physisorbed xenon for the x-HP samples.
- Fig. 3: Temperature dependent ^{129}Xe NMR chemical shifts of the resonances assigned to physisorbed xenon for the x-LP samples.
- Fig. 4: Temperature dependent ^{129}Xe NMR linewidths. Full triangles, 2-HP, resonance assigned to xenon within the pores, unfilled triangles, 2-HP, resonance assigned to xenon in between the cylindrical pores; filled circles, 1-HP, resonance assigned to xenon within the pores.
- Fig. 5: Ratio of the integral of the resonance assigned to xenon inside the pores over the gas resonance (filled circles) and liquid resonance (unfilled circles) for sample 1-HP. The inset shows the continuous increase in total signal intensity with decreasing temperature. Integrals were obtained from the data shown in Figure 1.
- Fig. 6: The data points (circles, 1-HP; triangles, 2-HP) were obtained by linear extrapolation of the temperature dependent chemical shifts of 1,2-LP and 1,2-HP to zero pressure. The dashed (silica 1) and solid (silica 2) lines represent fits to equation (1) for $m = 2$. The results of the fits are summarized in Table 4.

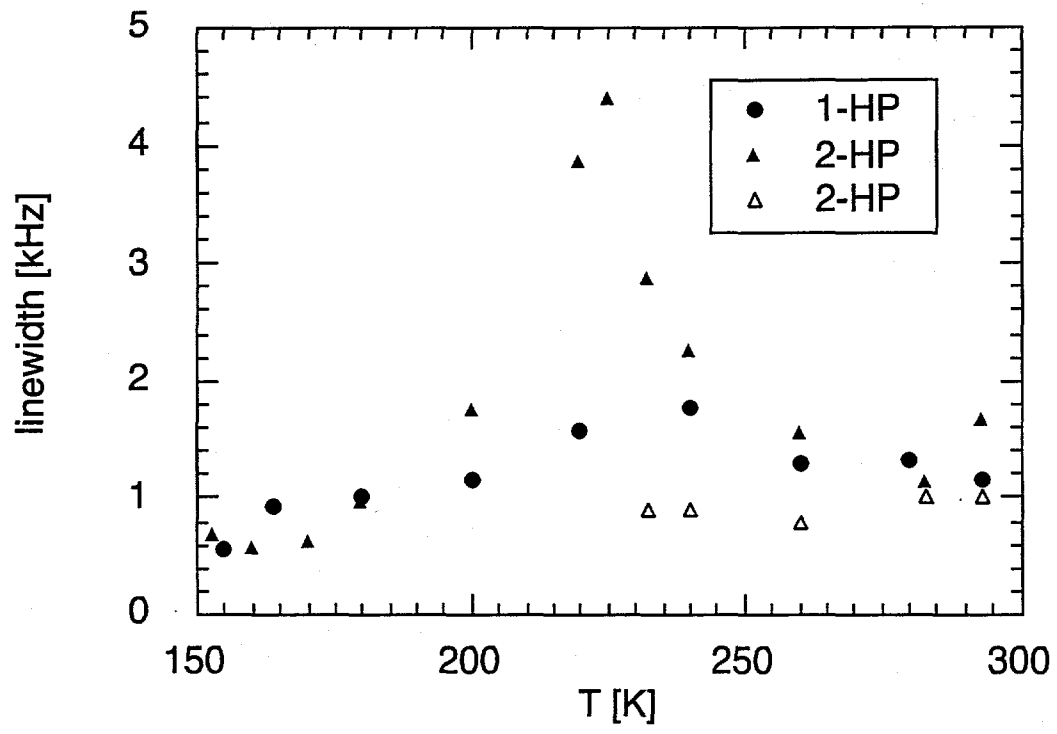




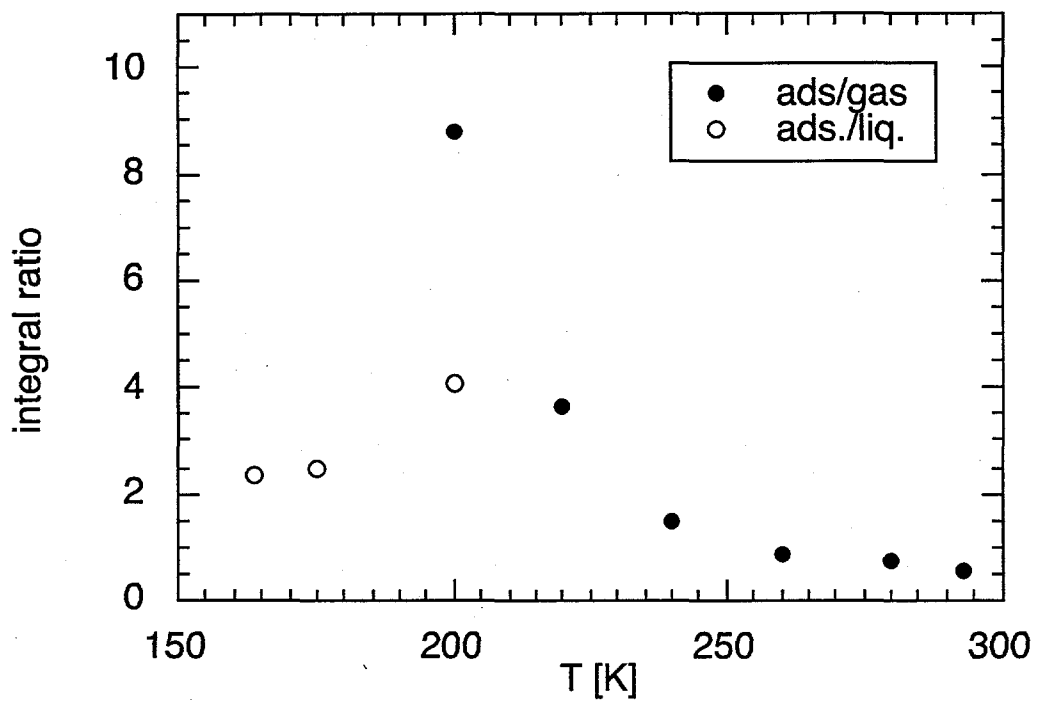
T. Pietraß et al.
figure 2



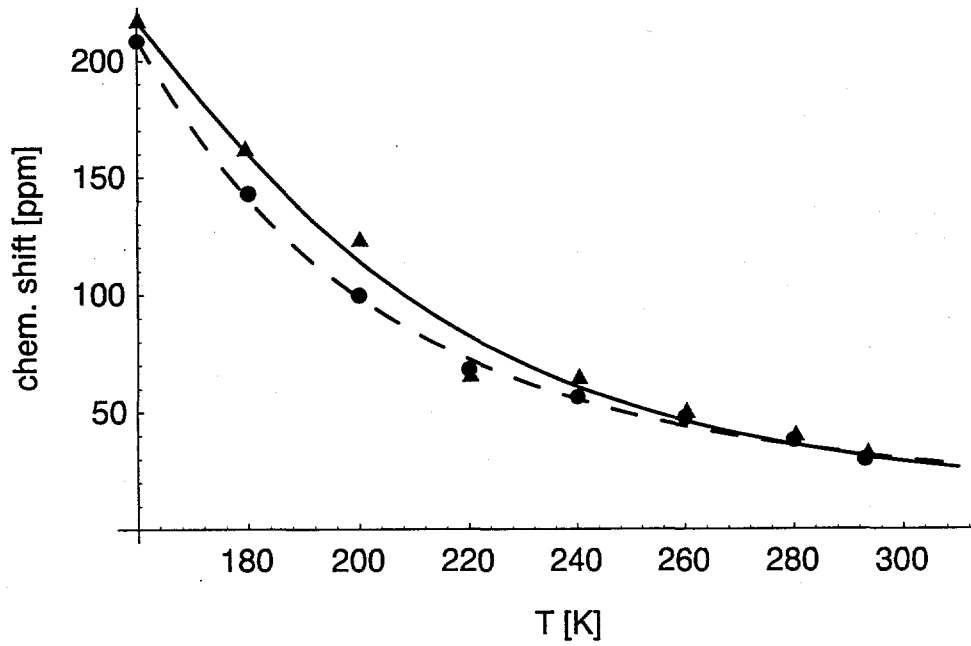
T. Pietraß et al.
figure 3



T. Pietraß et al.
figure 4



T. Pietraß et al.
figure 5



T. Pietraß et al.
figure 6